



1 **Climate change is rapidly deteriorating the climatic signal in Svalbard glaciers**

2

3 Andrea Spolaor<sup>1,2</sup>, Federico Scotto<sup>3</sup>, Catherine Larose<sup>4</sup>, Elena Barbaro<sup>1,2</sup>, Francois Burgay<sup>5,2</sup>, Mats P.  
4 Bjorkman<sup>6</sup>, David Cappelletti<sup>7</sup>, Federico Dallo<sup>2</sup>, Fabrizio de Blasi<sup>1,2</sup>, Dmitry Divine<sup>8</sup>, Giuliano  
5 Dreossi<sup>1,2</sup>, Jacopo Gabrieli<sup>1,2</sup>, Elisabeth Isaksson<sup>8</sup>, Jack Kohler<sup>8</sup>, Tonu Martma<sup>9</sup>, Louise S. Schmidt<sup>10</sup>,  
6 Thomas V. Schuler<sup>10</sup>, Barbara Stenni<sup>2</sup>, Clara Turetta<sup>1,2</sup>, Bartłomiej Luks<sup>11</sup>, Mathieu Casado<sup>12</sup> and  
7 Jean-Charles Gallet<sup>8</sup>.

8

9 <sup>1</sup>CNR-Institute of Polar Science (ISP), Campus Scientifico, Via Torino 155, 30172, Venice-Mestre, Italy.  
10 <sup>2</sup>Department of Environmental Sciences, Informatics and Statistics, Ca' Foscari University, Venice, Italy  
11 <sup>3</sup>Institute of Atmospheric Sciences and Climate, ISAC-CNR. S.P Lecce-Monteroni km1.2, 73100 Lecce, Italy  
12 <sup>4</sup>Environmental Microbial Genomics, Laboratoire Ampère, CNRS, University of Lyon, France  
13 <sup>5</sup>Paul Scherrer Institute, Laboratory of Environmental Chemistry (LUC), 5232 Villigen PSI, Switzerland  
14 <sup>6</sup>University of Gothenburg, Department of Earth Sciences, Box 460, 40530 Göteborg, Sweden  
15 <sup>7</sup>Dipartimento di Chimica, Biologia e Biotecnologie, Università degli Studi di Perugia, 06123 Perugia, Italy  
16 <sup>8</sup>Norwegian Polar Institute, Tromsø NO-9296, Norway  
17 <sup>9</sup>Department of Geology, Tallinn University of Technology, Ehitajate tee 5, 19086 Tallinn, Estonia  
18 <sup>10</sup>University of Oslo, Department of Geosciences, Oslo, Norway  
19 <sup>11</sup>Institute of Geophysics, Polish Academy of Sciences, Księcia Janusza 64, 01-452 Warsaw, Poland  
20 <sup>12</sup>Laboratoire des Sciences du Climat et de l'Environnement, CEA–CNRS–UVSQ–Paris-Saclay–IPSL, Gif-  
21 sur-Yvette, France  
22

23 Corresponding author: andrea.spolaor@cnr.it

24

25

26

27

28

29

30

31

32

33

34

35

36

37

38

39



40

#### 41 **Abstract**

42 The Svalbard archipelago is particularly sensitive to climate change due to the relatively low altitude  
43 of its main ice fields and its geographical location in the higher North Atlantic, where the effect of  
44 the Arctic Amplification is more significant. The largest temperature increases have been observed  
45 during winter, but increasing summer temperatures, above the melting point, have led to increased  
46 glacier melt. Here, we evaluate the impact of this increased melt on the preservation of the oxygen  
47 isotope signal ( $\delta^{18}\text{O}$ ) in firn records.  $\delta^{18}\text{O}$  is commonly used as proxy for past atmospheric  
48 temperature reconstructions and, when preserved, it is a crucial parameter to date and align ice cores.  
49 By comparing four different firn cores collected in 2012, 2015, 2017 and 2019 at the top of the  
50 Holtedahlfonna ice field (1100 m. a.s.l.), we show a progressive deterioration of the isotope signal  
51 and we link its degradation to the increased occurrence and intensity of melt events. Although the  
52  $\delta^{18}\text{O}$  signal still reflects the interannual temperature trend, more frequent melting events may in the  
53 future affect the interpretation of the isotopic signal, compromising the use of Svalbard ice cores. Our  
54 findings highlight the impact and the speed at which Arctic Amplification is affecting Svalbard's  
55 cryosphere.

56

#### 57 **Introduction**

58 Arctic regions are undergoing faster warming than the global average, due to the so-called “Arctic  
59 Amplification” (Dahlke et al., 2020). Arctic Amplification is caused by various feedback processes  
60 in the atmosphere-ocean-ice system and significantly affects the Arctic North Atlantic region. Arctic  
61 warming is not seasonally uniform and has the largest impact in the winter months and close to the  
62 surface (Rantanen et al., 2022a; Dahlke and Maturilli, 2017). Furthermore, it is not evenly  
63 distributed across the Arctic; the largest warming rates are over the Barents/Kara Seas, where autumn  
64 and winter sea-ice retreat is strongest (Lind et al., 2018; Isaksen et al., 2022, 2016). However, even  
65 at tropospheric levels, there is a significant warming signal in recent decades that peaks in the  
66 Svalbard region, and more generally, in the North Atlantic sector of the Arctic (Dahlke and Maturilli,  
67 2017). Rates there are up to four times the global average since 1979 (Rantanen et al., 2022b).  
68 Glaciers and ice caps in the Svalbard archipelago cover an area of  $\sim 34,000 \text{ km}^2$ , representing about  
69 6% of the world's glacier area outside the Greenland and Antarctic ice sheets. Svalbard glaciers  
70 contain  $7740 \pm 1940 \text{ km}^3$  (or Gigaton; Gt) of ice, sufficient to raise global sea level by  $1.7 \pm 0.5 \text{ cm}$   
71 totally melted (Schuler et al., 2020; Geyman et al., 2022; van Pelt et al., 2019) and are experiencing  
72 among the fastest warming on Earth (Noël et al., 2020) as a result of Arctic Amplification, and being  
73 situated at the edge of retreating Arctic sea ice.



74 Ongoing climate trends also affect the state of the seasonal snowpack in Svalbard (Østby et al., 2017;  
75 van Pelt et al., 2016). For example the numbers of days with snow-cover on the ground has decreased  
76 from 253 (1976-1997) to 219 (2006-2018). The change in the Svalbard climate has strong  
77 repercussions for the entire environment of the archipelago. For example, there has been an increase  
78 in frequency of Rain on Snow (RoS) events (Wickström et al., 2020) which lead to pervasive ice  
79 layers (Sobota et al., 2020) covering the ground, limiting access to food for reindeers (Peeters et al.,  
80 2019). The reduction in sea ice is limiting and changing the hunting area of polar bears. From a  
81 climate perspective, the transformation from one regime to another is gradual and requires centuries,  
82 as demonstrated by paleoclimatic studies, such as ice core investigations. Ice cores contain  
83 information about past climate conditions and atmospheric composition including traces of natural  
84 events (such as volcanic eruptions), past temperature reconstructions (Wolff et al., 2010) and  
85 anthropogenic contamination (Vecchiato et al., 2020). Such studies revealed that rapid climate  
86 changes have occurred in the past. For example, during the last glacial period in the Arctic, the so-  
87 called Dansgaard-Oeschger events occurred when temperatures rose by about 5°C (Boers, 2018).  
88 However, even during these natural abrupt events, a complete transition from stadial (glacial) to  
89 interstadial (warm) conditions took about a century (Scoto et al., 2022; Steffensen et al., 2008).  
90 Current temperature rise in Svalbard is much faster than the one observed during the D-O events,  
91 with annual mean surface air temperature increasing in average by  $+1.3 \text{ K} \pm 0.7 \text{ K}$  per decade, and  
92 winter mean temperature increasing by  $+3.1 \pm 2.4 \text{ K}$  per decade (Dahlke et al., 2020; Maturilli et al.,  
93 2013).  
94 (Vance et al., 2016; Spolaor et al., 2016). Snowmelt and water percolation at the sampling site can  
95 move the chemical constituents across the layers (Spolaor et al., 2021; Avak et al., 2019) disturbing  
96 the original signal. Prolonged events can even fully compromise the preservation of the climatic  
97 information contained by ice cores. Avak et al. (2019) showed that atmospheric composition was  
98 well preserved in an Alpine ice core during the winter, but that the melting in the spring and early  
99 summer caused a preferential loss of certain major ions and trace elements. In particular, the elution  
100 behavior of major ions is most likely controlled by redistribution processes occurring during snow  
101 metamorphism, as underlined by recent work investigating the distribution of impurities within the  
102 ice matrix (Bohleber et al., 2021). Variable mobility has also been observed for trace elements,  
103 although they have been suggested to be better preserved than major ions. The Antarctic and the  
104 Greenland plateau are the best locations for such studies, since the temperature is below the melting  
105 point ( $<0^\circ\text{C}$ ), although rare melting events occur in the Greenland plateau (Bonne et al., 2015).  
106 However, ice cores retrieved from these locations do not provide more regional climatic information.  
107 To overcome this limitation, many other drilling sites have been investigated, for example in the Alps



108 (Arienzo et al., 2021; Gabrielli et al., 2016; Schwikowski et al., 1999) the Himalayas (Thompson et  
109 al., 2018; Dahe et al., 2000), the Andes mountain range (Hoffmann et al., 2003), the Canadian  
110 Arctic (Zdanowicz et al., 2018) and the Svalbard archipelago (Isaksson et al., 2005; Wendl et al.,  
111 2015).

112 There are several ice caps in Svalbard, but given their relatively low altitude, most are not suitable  
113 for the preservation of a pristine climate archive. The glacier equilibrium line altitude (ELA) varies  
114 across the different regions of the archipelago but is generally situated between 300 to 700 m a.s.l. (van  
115 Pelt et al., 2019). In the southern part of the archipelago, the ELA is lower due to the higher winter  
116 snow accumulation, while in the northern part, the ELA rises to 600-700 m. Signal preservation  
117 requires drilling to be above the ELA, for regular snow accumulation, but also, so that summer  
118 percolation only moderately affects the upper firn layers.

119 Several drilling operations have collected ice core records in the archipelago, in particular in the  
120 northern part. The longest (in time coverage) ice-core record was collected from Lomonosovfonna,  
121 at 1230 m a.s.l., and covered ~1200 years of Svalbard climate history (Divine et al., 2011). Other ice  
122 cores have been collected from Austfonna (750 m. a.s.l.), covering approximately 900 years  
123 (Watanabe et al., 2001), Vestfonna (600 m a.s.l.) covering approximately 500 years (Matoba et al.,  
124 2002) and Holtedahlfonna (1140 m a.s.l.) covering approximately 300 years (Beaudon et al., 2013).

125 To evaluate the robustness of Svalbard ice cores for future climate studies, we analysed the oxygen  
126 isotopic composition ( $\delta^{18}\text{O}$ ) of a sequence of four shallow ice cores collected at the top of the  
127 Holtedahlfonna ice field in different years, each covering an overlapping atmospheric deposition  
128 period, to provide a view of the evolution of isotopic stratigraphy over time. We focalize our study  
129 on the  $\delta^{18}\text{O}$  since is the parameter most used in the ice core science for reconstruct the past  
130 temperature change (Divine et al., 2011; Stenni et al., 2017) and it is one of the less affected, compare  
131 to the other chemical parameters analyzed in ice core, by the melting and percolation events (Pohjola  
132 et al., 2002). Several studies dealing with different elements and compounds have already been  
133 performed using shallow cores from the summit of the Holtedahlfonna ice field, demonstrating the  
134 importance of the site for climate studies (Burgay et al., 2021; Barbaro et al., 2017; Spolaor et al.,  
135 2013a; Ruppel et al., 2017). Results were linked to glacier mass balance measurements and snowpack  
136 modelling. Based on our results, we observed that the climate signal is progressively deteriorating,  
137 although the long term (>5 years) climate variation still seems preserved. This underscores the  
138 urgency for obtaining records to help understand the climate processes occurring in one of the fastest  
139 changing environments on Earth.

140

## 141 **2. Methodology**



142 **2.1 The Holtedahlfonna ice field**

143 Holtedahlfonna (HDF – Figure 1) is the largest ice field (ca. 300 km<sup>2</sup>) in northwestern Spitsbergen,  
144 located about 40 km from the Ny-Ålesund research station. It covers an elevation range of 0–1241 m  
145 a.s.l. (Nuth et al., 2017) and the upper part of the glacier, located approximately at 1100 m a.s.l., has  
146 a positive annual snow mass balance, ca. +0.50 m. w.e. a<sup>-1</sup> (Beaudon et al., 2013; van Pelt et al., 2019).  
147 The site has already been studied for long term paleoclimate reconstruction, covering the past 300  
148 years (Divine et al., 2011; Goto-Azuma et al., 1995). In April 2005, a 125 m a long ice core was  
149 drilled using an electromechanical corer and the bottom temperature in the borehole was –3.3°C,  
150 assuring cold ice conditions over the entire ice thickness. Ice temperature measured in the borehole  
151 featured a maximum of –0.4°C at 15 m depth, indicative of firn-warming due to the release of latent  
152 heat from refreezing (Beaudon et al., 2013).

153

154 **2.2 The Holtedahlfonna shallow firn cores: collection and processing**

155 In the spring seasons of 2012, 2015, 2017 and 2019, a total of four shallow cores were obtained from  
156 the summit of the Holtedahlfonna ice field (79°09'N, 13°23'E; 1150 m. a.s.l.). The shallow cores were  
157 collected using a 4" fiberglass Kovacs Mark-II ice corer driller powered by an electric drill and  
158 reached depths of 7-10 m into the firn. All shallow cores were drilled from the bottom of the annual  
159 snowpack\last summer surface. Length and density of each firn core section were logged, stored in  
160 plastic sleeves, and transported back to Ny-Ålesund for laboratory analysis. For cores collected in  
161 2012, 2017 and 2019, core samples were processed in a class-100 laminar flow hood in the laboratory  
162 of the Italian research station “*Dirigibile Italia*” in Ny-Ålesund. Core sections were cut into pieces of  
163 5 to 7 cm length using a ceramic knife and the external part of the core physically removed to avoid  
164 contamination. The density was measured for each sample produced. The core 2015 was processed  
165 as reported in Ruppel et al. (2017).

166

167 **2.3 Oxygen stable isotope analysis ( $\delta^{18}\text{O}$ )**

168 The samples for oxygen isotopic analyses ( $\delta^{18}\text{O}$ ) were melted at room temperature ( $\approx 20^\circ\text{C}$ ) and  
169 transferred into 2-mL clear glass vials filled to the top. Samples were kept refrigerated at +4°C and  
170 analyzed at Ca Foscari University of Venice (2017 and 2019) and at Tallinn University of Technology  
171 (2012 and 2015). In both cases, the isotopic measurements were carried out using a Picarro L1102-*i*  
172 analyser coupled with a CTC Pal autosampler. The instrument uses Cavity Ring-Down Spectroscopy  
173 (CRDS) technology, based on the unique near-infrared absorption spectrum of each gas-phase  
174 molecule. The autosampler injects the melted sample into the vaporizer (set at 110°C), where it  
175 becomes gaseous and is then transferred into the cavity (nitrogen is used as a carrier), in which the  
176 measurement occurs. The instrument datasheet reports an analytical precision of  $\pm 0.10$  ‰ for  $\delta^{18}\text{O}$ .



177 Each sample was injected eight times: only results within  $\pm \sigma$  from the 8-repetition average were kept  
178 for records, while outliers were discarded. Internal isotopic standards periodically calibrated against  
179 IAEA-certified standards (V SMOW 2 and SLAP 2) were used for calibration.

180

#### 181 **2.4 Holtedahlfonna surface mass balance**

182 Surface mass balance (SMB) of Holtedahlfonna is monitored by the Norwegian Polar Institute  
183 (Kohler, 2013). SMB is obtained from repeated field visits at the end of winters and summers, with  
184 winter snow-depth sounding and density measurements and repeated height readings of an array of  
185 stakes along the glacier centerline. Balance estimates are extrapolated over the entire glacier basin by  
186 determining the balance as function of elevation and averaging them, applying weights determined  
187 from the distribution of glacier area as a function of elevation. This method quantifies the glacier-  
188 wide SMB, i.e., the mass changes at the surface of the glacier, and within near-surface layers, but  
189 does not include internal mass changes below the last summer surface. SMB measurements at  
190 Holtedahlfonna started in 2003; since the drilling site is in the accumulation area, these measurements  
191 provide information of the seasonal accumulation, but disregard the internal accumulation that may  
192 occur due to refreezing of meltwater in layers below the last summer surface. The uppermost part of  
193 the Holtedahlfonna (HDF) has had a consistently positive mass balance and is therefore assumed to  
194 preserves most of its annual snow deposition.

195

#### 196 **2.5 Estimation of Meteorological condition at the summit of the Holtedahlfonna ice field**

197 In absence of in-situ meteorological measurements at the drill site, we obtained long-term seasonal  
198 (DJF, MAM, JJA and SON) temperature and precipitation series from the high-resolution CARRA  
199 dataset (Copernicus Arctic Regional Re-Analysis, Schyberg et al., 2020). This 2.5 km resolution  
200 product covering the period 1991-2020 is downscaled from ERA5(Hersbach et al., 2020) using the  
201 state-of-the-art weather prediction model HARMONIE-AROME (Bengtsson et al., 2017). CARRA  
202 has several improvements compared to ERA5, including assimilation of a large amount of additional  
203 surface observations, extensive use of satellite data, and improved representation of sea ice; it is  
204 therefore likely to provide the best estimate of meteorological conditions in the Barents Sea region.  
205 The CARRA reanalysis is also used to force the CryoGrid community model (Westermann et al.,  
206 2023) to simulate glacier mass balance, seasonal snowpack evolution and meltwater runoff across  
207 Svalbard Franz-Joseph Land and Novaya Zemlya. The model couples the surface energy balance and  
208 a multi-layer subsurface module to resolve meltwater production, percolation, storage, refreezing and  
209 runoff, accounting for the interaction with local density and temperature stratigraphers. The vertical



210 discretization comprises 47 layers of variable vertical extend to cover the uppermost 20 m below the  
211 surface (Steffensen Schmidt et al., 2023).

212

### 213 **3.RESULTS**

#### 214 **3.1 Shallow firn core dating and alignment**

215 To date the core, we use the seasonal cycle (where present) of the  $\delta^{18}\text{O}$  data together with the mass  
216 balance data available since 2003. Core depths were converted to water equivalent using the density  
217 data acquired during the core processing. Density for the 2015 core is taken from Ruppel et al., (2017),  
218 the 2012 values are published in Spolaor et al., (2013b), and density for the 2017 and 2019 cores are  
219 presented in this work; density profiles of the four shallow cores (Figure S1) all reveal a similar  
220 pattern.

221 The cores were collected within 50 m of the mass balance stake HDF-10. The stake measurements,  
222 which show a consistently net positive mass balance, provide a historical record of snowpack  
223 accumulation that can be directly used to assign a specific year to firn core depth range (Figure 2).

224 Oxygen stable isotopes ( $\delta^{18}\text{O}$ ) can be used independently to annually date the ice, but only in ice-  
225 core archives where the seasonal signal is well preserved. This means that snow accumulation needs  
226 to be sufficiently high, and the summer ablation should not compromise the stratigraphy by  
227 redistributing and smoothing the original atmospheric signal. By combining the annual accumulation  
228 and the core depth expressed in water equivalent and the seasonality of  $\delta^{18}\text{O}$  (where available and  
229 preserved), we can date and align all four cores (Figure 3).

230 The cores cover 14 years (2004 to 2018). The time coverage for each core is reported in Table 1  
231 together with additional information for each firn core. The 2012 core had a  $\delta^{18}\text{O}$  average value of -  
232  $15.3 \pm 1.0$  ‰, the 2015 core a value of  $-15.1 \pm 0.8$  ‰, the 2017 core an average value of  $-14.4 \pm 0.7$   
233 ‰ and the 2019 core an average value  $-14.1 \pm 1.2$  ‰. The cores have a good overlap (Figure 3 and  
234 6), and show a general increasing trend in  $\delta^{18}\text{O}$  from 2004 until 2018. In particular, the 2012 and  
235 2015 cores have similar trends, particularly during 2005-2006, a feature also useful for core  
236 alignment. They also showed similar trends in the remaining periods that they each covered, though  
237 with minor differences. The high values in  $\delta^{18}\text{O}$  determined in year 2013 in the 2015 core are also  
238 clearly found in the 2017 core, helping to synchronize the records. The alignment of the 2019 core  
239 with previous cores could only be done through mass balance values, since the  $\delta^{18}\text{O}$  values did not  
240 show the same peaks as the other records. In particular, the decrease in  $\delta^{18}\text{O}$  values recorded in the  
241 period representing 2016 was not present in the 2017 core.

242

#### 243 **3.2 Meteorological condition at the Holtedahlfonna ice field summit**



244 The meteorological conditions at the Holtedahlfonna ice field summit from 1991 to 2020 were  
245 retrieved from model re-analysis and provide a clear overview of the on-going changes occurring at  
246 the site.

247 The annual average winter temperatures (DJF) at the HDF summit (located at 1100 m a.s.l.) ranged  
248 from  $-25^{\circ}\text{C}$  to  $-15^{\circ}\text{C}$ , and show an increasing trend of  $2.37^{\circ}\text{C}$  per decade for the period 1991–2020  
249 (Figure 4a - blue line). The annual average spring and summer temperatures (MAM) ranged from -  
250  $17^{\circ}\text{C}$  to  $-12^{\circ}\text{C}$  (Figure 4a - green line) and  $-5^{\circ}\text{C}$  to  $-1^{\circ}\text{C}$  (Figure 4a - red line), respectively. The  
251 average temperature increase per decade since 1991 was  $0.38^{\circ}\text{C}$  for spring and  $0.51^{\circ}\text{C}$  for summer.  
252 The temperature during fall (SON) increased by  $1.47^{\circ}\text{C}$  per decade and ranged from  $-15^{\circ}\text{C}$  and  $-5^{\circ}\text{C}$   
253 (Figure 4a - brown line).

254 Although the average seasonal summer temperatures were below the water melting point, positive  
255 degree days (PDD – Figure 4b, expressed as the sum of mean daily temperatures for all days during  
256 a period where the temperature is above  $0^{\circ}\text{C}$ ), occurred at the summit of HDF, causing snowpack  
257 melting. The cumulative annual PDD, retrieved from model temperature series outputs, showed a  
258 stable value for the period 1990 to 2015, although some years (1994, 1999, 2010) and periods (2001–  
259 2006) were characterized by an increased PDD. A net increase from 2015 to the present time was  
260 recorded. Snow melting at the site was clearly visible and confirmed by the presence of several ice  
261 lenses in the core (Spolaor et al., 2013b; Burgay et al., 2021).

262 The annual model estimated precipitation (1991–2020) ranged between 630 to 1170 mm w.e. per  
263 year, with a slight increase in the most recent period (Figure 4d). A similar trend was also observed  
264 in Ny-Ålesund (Førland et al., 2020). Seasonal precipitation (Figure S2) was most abundant during  
265 fall (SON) and winter (DJF), with an average precipitation of 286 mm w.e. and 274 mm w.e.,  
266 respectively, and a relative average contribution of 32% and 31%, respectively, to the total deposition.  
267 The lowest precipitation occurred in spring (MAM) and summer, with an average precipitation of  
268 170 mm w.e. and 145 mm w.e., respectively, which represents an average contribution of 20% of the  
269 total deposition in spring and 17% of the total precipitation in summer.

270 Although the annual mass balance was always positive, the summer mass balance was both positive  
271 and negative depending on the meteorological conditions (Figure 2). The winter accumulation  
272 represented between 60% and 100% of the net annual mass balance at the site. Even though the  
273 summer mass balance data from 2015 to 2020 were positive, melting also occurred and water  
274 percolated into the snow and firn before refreezing.

275 Most of the melting occurred during the summer period (JJA), but melting events also occurred during  
276 fall and late spring (Figure S3). The estimated annual melting at the site from 1991-2020 (Figure 4c)  
277 varied between 960 mm w.e (2020) and 117 mm w.e (2008) and showed a clear increasing tendency





278 following temperature rise. Moreover, autumn snowpack melting events, previously rare, became a  
279 more regular phenomenon in the period 2015 to 2019. However, spring snowmelt is sporadic (2011)  
280 and rare.

281 In addition to meteorological reanalysis from the HARMONIE-AROME model, the CryoGrid  
282 simulation provided information about the presence of liquid water in the firn and its penetration  
283 (Figure 5). Percolation was mainly confined to the surface layer between 1991 (beginning of the  
284 simulation) to the end of the 90s(except 1999). Percolation increased significantly from 2000  
285 onwards. In particular, for the period 2004-2005, severe surface melt events occurred (Figure 2c and  
286 Figure S3), causing water percolation for several meters (Figure 5). The 2006 to 2014 period was  
287 characterized by relatively limited surface melting and the lowest amount of percolated water, which  
288 did not exceed one (2006 and 2008) to four (2010 and 2011) annual snow accumulation periods.  
289 Based on the model's calculations, water percolation increased since 2014 and was able to reach  
290 deeper firn strata. Although the model suggests the presence of liquid water in the firn, water and  
291 elution channels are complex to simulate and likely present high spatial variability. Hence, we only  
292 consider the data presented in Figure 5 in a qualitative manner to evaluate the possible presence or  
293 absence of liquid water within the snowpack and its theoretical penetration/percolation depth.

294

#### 295 4. DISCUSSION

296 The aim of the paper is to evaluate the effect of temperature rise on the  $\delta^{18}\text{O}$  Høltedahlfonna ice core  
297 signal preservation. Our discussion will focus only on the periods covered by the shallow cores.

298 Based on the  $\delta^{18}\text{O}$  records of the four shallow cores, it is evident that the seasonal signal experienced  
299 considerable changes and progressively deteriorated in the most recent cores. The most important  
300 parameters affecting the pristine atmospheric signal trapped in the snow is the amount of snow  
301 melting, which depends on the snow and meteorological conditions, and the penetration of the melt  
302 water into the snowpack.

303 In the core collected in 2012 (Figure 3), the seasonal variations are clear for almost the entire period  
304 except for 2004-2005, a period characterized by significant summer melt that disturbed the  
305 atmospheric signal trapped in the ice. However, for the period 2006-2011, the seasonality is clear and  
306 each  $\delta^{18}\text{O}$  seasonal cycle is confined within the annual snow mass balance measurements.

307 The 2015 core still presented the seasonal cycle in the upper half of the core, corresponding to the  
308 second period (2010-2014). However, the seasonal feature of the  $\delta^{18}\text{O}$  identified in the core 2012 for  
309 the periods 2008–2009 was no longer present, suggesting a possible elution caused by the percolation  
310 of liquid water (Figure 5). The model simulation supports the possibility that post deposition events  
311 may have occurred within the firn due to the percolation of liquid water.



312 The most striking change in terms of the  $\delta^{18}\text{O}$  seasonal cycle occurred in the 2017 core. The 2017  
313 core overlapped with the 2015 core for the period 2012-2014 and, while the seasonality for this period  
314 was well defined in the 2015 core, only the seasonal  $\delta^{18}\text{O}$  for year 2013 was visible in the 2017 core.  
315 The  $\delta^{18}\text{O}$  seasonal cycle of 2014 has undergone significant smoothing and the  $\delta^{18}\text{O}$  seasonal cycle in  
316 2012 is no longer visible. For the period 2015-2016, the seasonal cycle was not clear, although  
317 oscillations were still present.

318 In the most recent core collected in 2019, a seasonal  $\delta^{18}\text{O}$  cycle could no longer be detected and  
319 particular features, such as the drop in the  $\delta^{18}\text{O}$  signal in 2016 (not observed in the 2017 core), was  
320 not linked to a drop in the temperature, since 2016 was the warmest year on record (Figure 6, red  
321 dots).

322 Two independent statistical analyses, one using the significant value of a regression model and the  
323 other using the spectral analysis, were performed on the shallow core records to test the presence of  
324 seasonal oscillation on the  $\delta^{18}\text{O}$  signal. Both statistical analyses demonstrated the disappearance of  
325 the seasonal signal in the most recent (2017 and 2019) shallow cores (full details are reported in the  
326 supplementary material - section 2).

327 The change in seasonality and, to a lesser extent, in the total amount of precipitation, might have  
328 influenced the  $\delta^{18}\text{O}$  signal of the four cores. However, from the model results, the seasonal  
329 contribution to the total annual precipitation did not change significantly (Figure S2). This would  
330 suggest that precipitation does not play a central role in explaining the degradation, or possible  
331 change, in the  $\delta^{18}\text{O}$  signal, and that increased melting and water percolation might have had a larger  
332 effect. Instead, the increase in year-round precipitation could enhance melt water formation during  
333 the summer periods. The preservation of the ice core climate signal strongly depends on the amount  
334 of snow melt during summer and the capability of water to penetrate the snowpack, which in turn is  
335 controlled by snow temperature. The progressive atmospheric warming, the increase of summer  
336 melting and water percolation as well as the water movement within the snowpack could all have had  
337 an impact on the  $\delta^{18}\text{O}$  signal present in the Høltedahlfonna firn\ice.

338 The progressive degradation and loss of the seasonality of the  $\delta^{18}\text{O}$  signal in the shallow core (2004-  
339 2018) is also supported by the results obtained from the  $\delta^{18}\text{O}$  signal in the 2005 core. In the deep core  
340 collected in 2005, the seasonal signal of the  $\delta^{18}\text{O}$  in the period 1960 to 2000 was well preserved  
341 (Figure S5). The signal determined in the 2005 Høltedahlfonna deep ice core shared similar features  
342 with those determined in the 2012 and 2015 shallow cores, where the seasonal oscillations were still  
343 partially present, but not with signals determined in the 2017 and 2019 cores, where the seasonality  
344 in  $\delta^{18}\text{O}$  almost disappeared. We suggest that since 2015, estimated melting and percolation increased



345 because of the evolution of the general atmospheric conditions, causing a deterioration of the climate  
346 signal preserved in the firn\ice.

347 Water stable isotopes are commonly used as a temperature proxy. By overlapping the water stable  
348 isotope profiles measured in the shallow cores and, comparing their trends with the annual average  
349 temperature, we suggest that the general atmospheric temperature trend is still preserved within the  
350 HDF ice (Figure 6), although some clear deterioration is visible. For example, the highest annual  
351 temperature values recorded in 2016 were not mirrored in the  $\delta^{18}\text{O}$  record from the 2017 and 2019  
352 cores. This underscores the impact of high temperatures on the preservation of pristine atmospheric  
353 signals in ice cores that have significantly impacted the preservation of the atmospheric signal, since  
354 temperature values.

355

## 356 **5. Conclusion**

357 An ice core drilled at the summit of Holtedahlfonna has previously been used to provide atmospheric  
358 and climate conditions about the past 300 years (Beaudon et al., 2013). Before 2005, the site was  
359 characterized by moderate summer melting, but the snow and ice was shown to preserve important  
360 climate information as well as the main seasonal features. The current warming of the Svalbard  
361 archipelago has clearly enhanced glacial mass loss, with a rise in the equilibrium line altitude and a  
362 shorter snow season. This study is the first investigating the impact of temperature rise on climate  
363 signal preservation within the firn\ice in one of the highest ice fields in Svalbard. The direct effect of  
364 higher temperatures has increased summer melt and enhanced meltwater percolation. In this study,  
365 we have shown that the climate signal preserved in the ice has been progressively deteriorated. For  
366 example, in seven years, the seasonal signal visible in the 2012 core has completely disappeared in  
367 the 2019 core, most likely due to increased snow summer melting and water percolation. However,  
368 although the  $\delta^{18}\text{O}$  seasonal signal has disappeared, the overall atmospheric warming signature is still  
369 preserved in the ice\firn, suggesting that the site is still suitable for long record paleoclimate  
370 reconstruction. However, with the current warming rate of the Svalbard archipelago and the  
371 consequent increase in summer melting, Holtedahlfonna and other ice fields at similar altitudes might  
372 no longer provide suitable records of the climatic condition. Glaciers worldwide are currently not  
373 only losing mass at unprecedented rates, but also the climatic information they contain.

374  
375  
376  
377  
378  
379  
380  
381



382 **Acknowledgments**

383 This work has been supported by the “Programma di Ricerca in Artico” (PRA, project number  
384 PRA2019-0011, Sentinel); by the Svalbard Science Forum/Research Council of Norway through the  
385 Arctic Field Grant call (project ASIHAD, ISSICOS, BIOMASS), by French Polar Institute IPEV  
386 (Institut Polaire Français Paul-Emile Victor) science funding (programs 399 and 1192) and the  
387 Svalbard Strategic Grant (project C2S3, nr. 257636, SnowNet nr. 295779 and BC3D nr. 283466).  
388 This project has received funding from the European Union's Horizon 2020 research and innovation  
389 programme under grant agreement no. 689443 via project iCUPE (Integrative and Comprehensive  
390 Understanding on Polar Environments). This research has been partially funded by the University of  
391 Perugia Research Action no. 5 “Climate, Energy, and Mobility”. Cryogrid simulations have been  
392 supported by the Nansen Legacy project (Research Council of Norway grant 276730) and SIOS  
393 infraNor (Research Council of Norway grant 269927).

394

395

396 **Author contribution**

397 AS, EB, FS, JCG, CL, MB, JG, FB, and DC conceived the experiment and collected the samples and  
398 wrote the paper with the support of all co-authors; CT, TM, GD and BS analyze the samples; JK  
399 provide the field mass balance data and contribute in data interpretation; LSS and TVS provide  
400 the model data and atmospheric re-analysis; FdB and MC perform the statistical exercise and  
401 contribute in data interpretation. BL and FD contribute to data interpretation. DD and EI  
402 provide the data from previous ice core and contribute to data interpretation.

403

404 **Data availability**

405 The data will be available upon request to the corresponding author.

406

407 **Competing interests**

408 The authors declare that they have no conflict of interest.

409

410

411

412

413

414

415

416

417

418

419

420

421

422

423



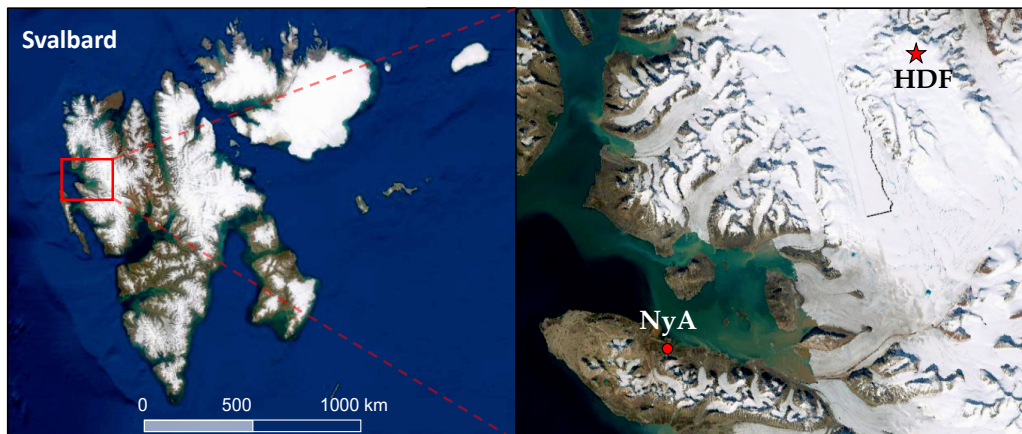
424 **FIGURES**

425

426 **Figure 1.** Location of the drilling site (red star) within the Holtedahlfonna (HDF) ice field as  
427 compared to the Ny-Ålesund research village (NyA). Maps from <https://toposvalbard.npolar.no> (last  
428 access: 5<sup>th</sup> June 2023).

429

430



431

432

433

434

435

436

437

438

439

440

441

442

443

444

445

446

447

448

449

450

451

452

453

454

455

456

457

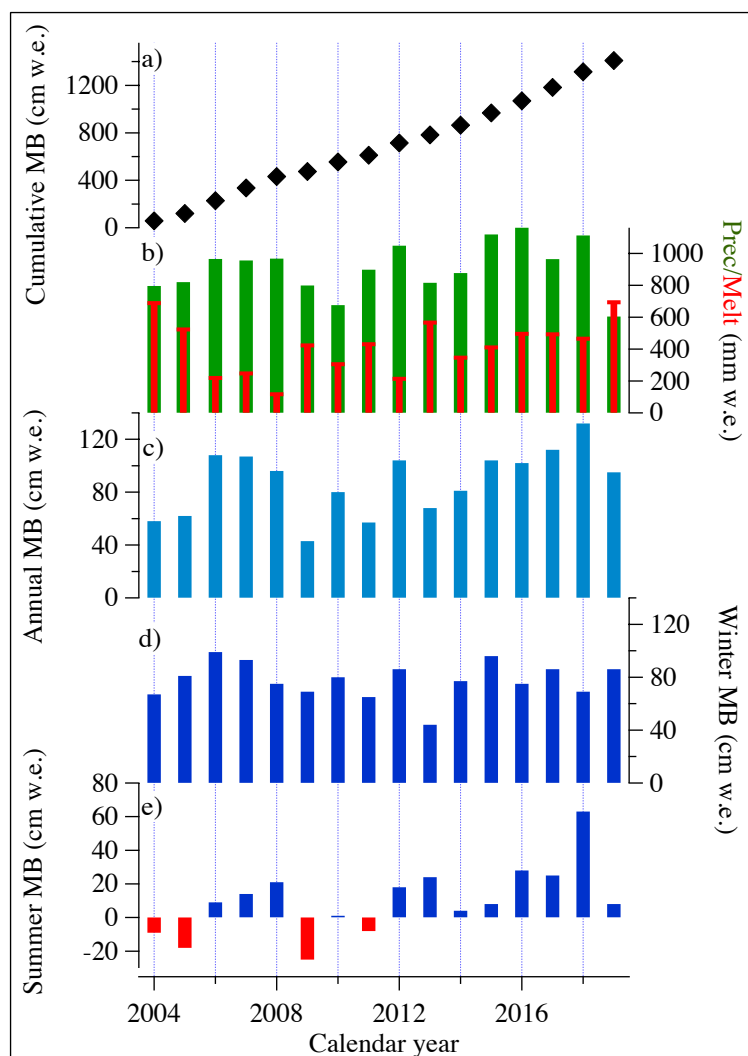
458

459

460



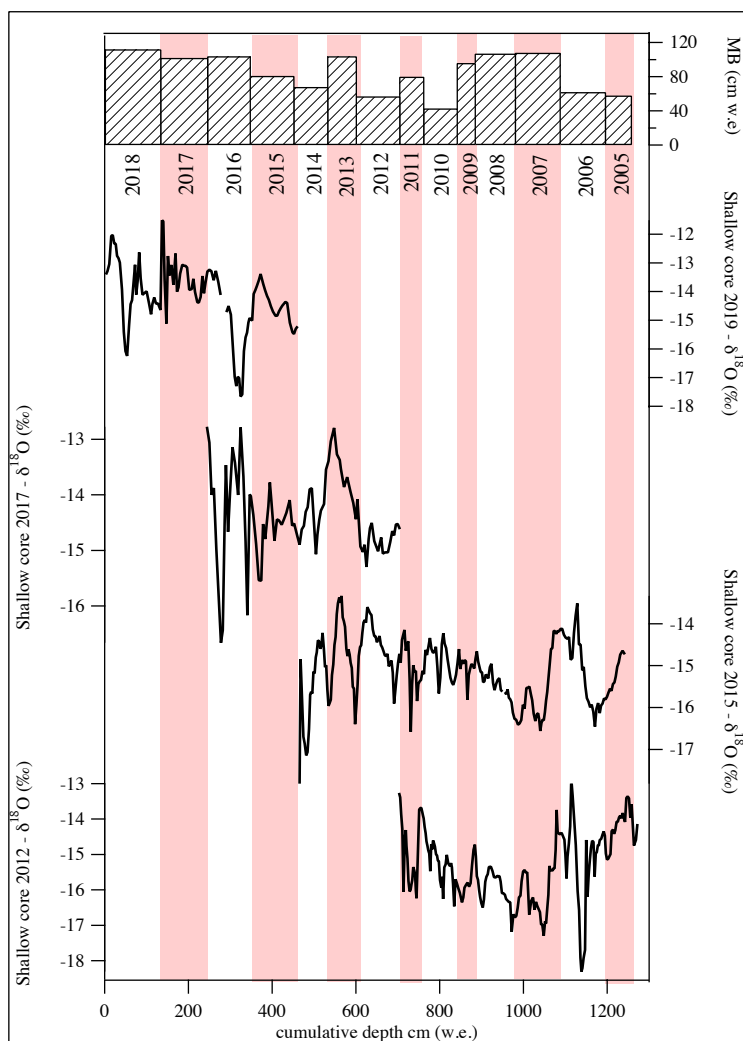
461 **Figure 2.** Mass balance measurements, modelled precipitation and snow melt at the drilling site. a)  
462 cumulative surface mass balance (SMB) expressed in cm of w.e., b) comparison of modeled total  
463 annual precipitation (green – in mm w.e) and modeled melt (red in mm w.e). c-e) net, winter and  
464 summer mass balance (cm w.e.) measured at the top of the Holtedahlfonna ice field, respectively.  
465  
466  
467



468  
469  
470  
471  
472  
473  
474  
475  
476



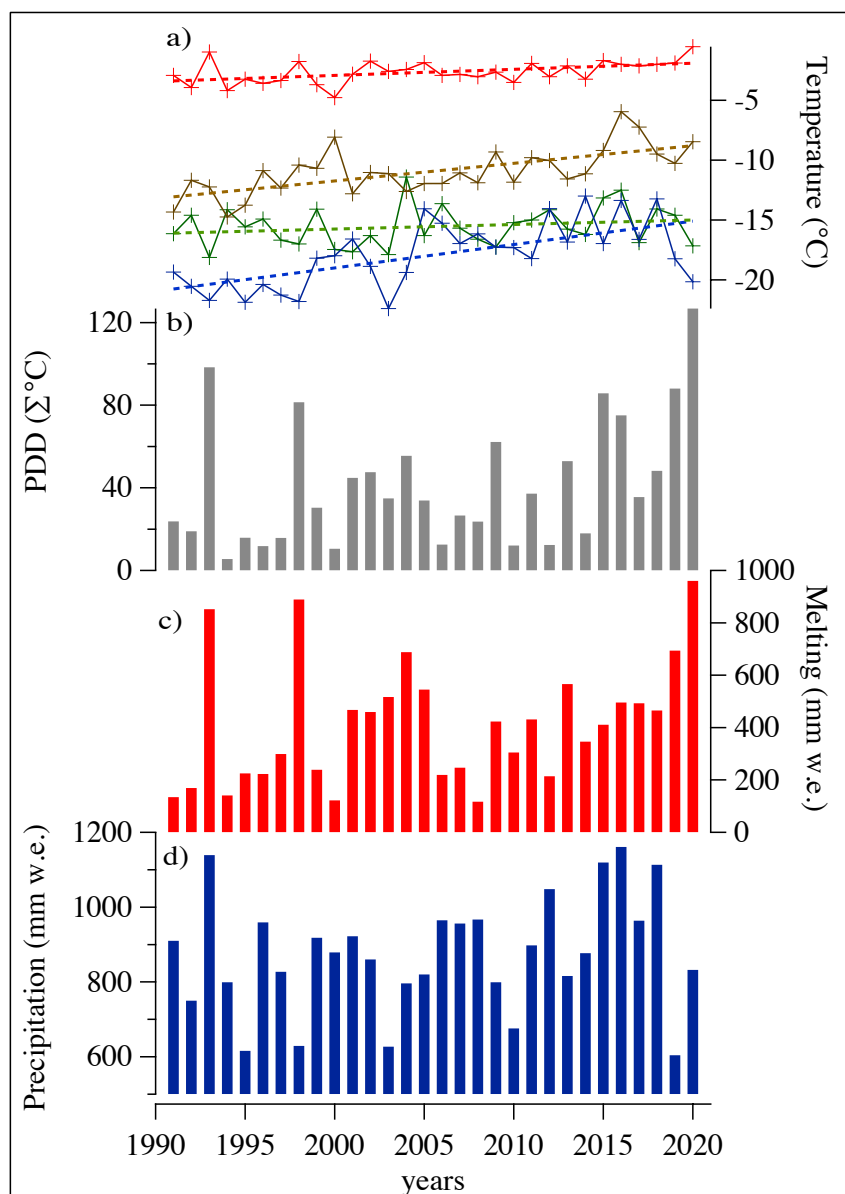
477 **Figure 3. Oxygen stable isotope profiles**  $\delta^{18}\text{O}$  of the shallow cores. The shallow core was aligned  
478 by converting the depth to depth expressed in cm of w.e. using the annual mass balance (MB) data.  
479 The white and pink colors distinguish different years based on the MB measurements and are reported  
480 in the upper panel.  
481



482  
483  
484  
485  
486  
487  
488  
489  
490  
491  
492  
493  
494  
495  
496  
497  
498  
499  
500  
501  
502  
503  
504  
505  
506  
507  
508  
509  
510  
511  
512  
513  
514  
515  
516  
517  
518  
519  
520  
521  
522  
523  
524  
525  
526  
527



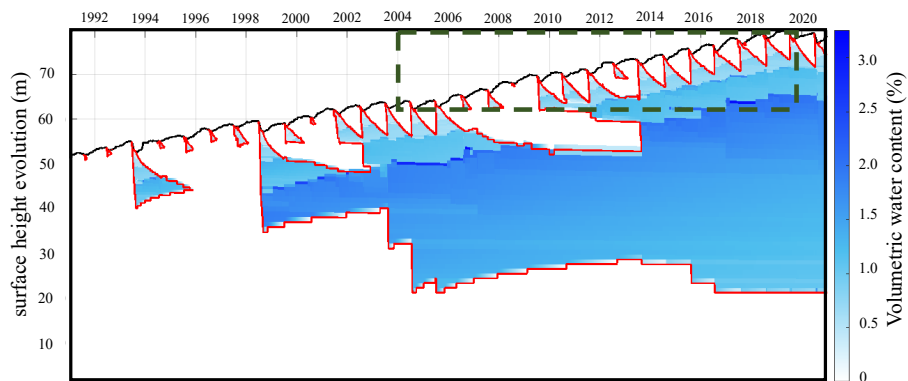
528 **Figure 4.** Modeled meteorological conditions at the Holtedahlfonna shallow core drilling site (1150  
529 m a.s.l.) from 1991 to 2020 at seasonal resolution. a) winter (DJF - blue), spring (MAM - green),  
530 summer (JJA - red) and fall (SON - brown) temperatures, with increasing trend line for the period  
531 investigated. b) annual PDD value (grey). c) annual melting (in mm w.e. in red). d) annual total  
532 precipitation (in mm w.e. - blue)  
533  
534







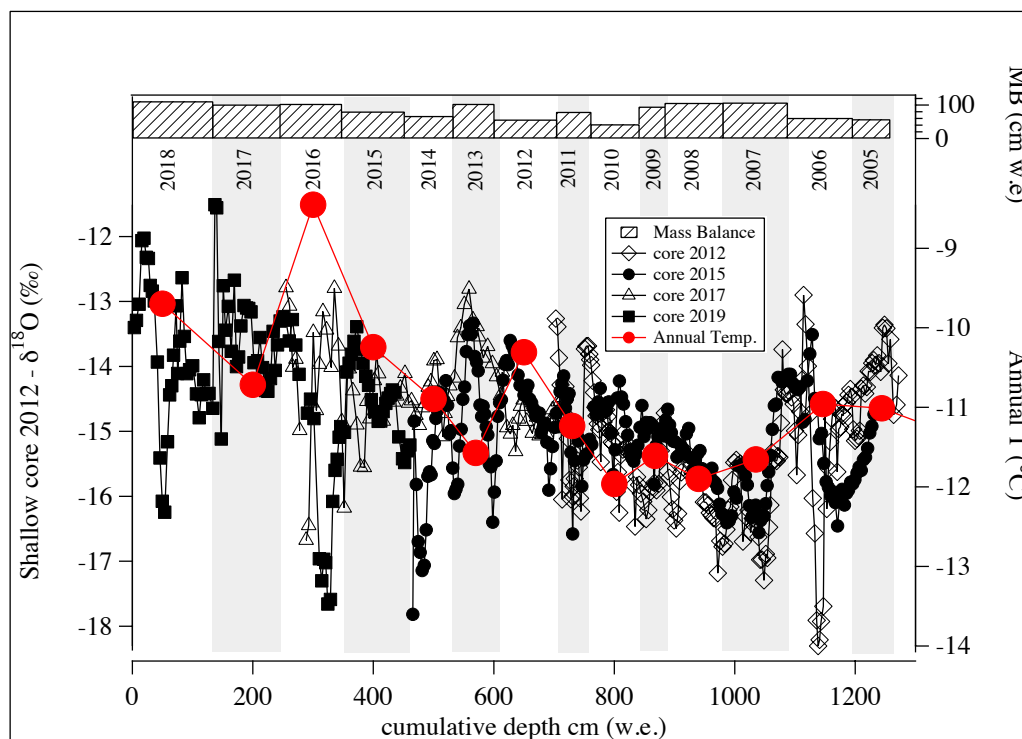
578 **Figure 5.** Evolution of the water content in the snowpack at the top of Holtedahlfonna estimated by  
579 model simulation between 1990 and 2020. The chart shows the volumetric water content (%) in the  
580 snow/firn (white to blue color), surface height evolution (black line), 0° C isotherm (red). Dashed  
581 lines show the period covered by the four shallow cores.  
582



583  
584  
585  
586  
587  
588  
589  
590  
591  
592  
593  
594  
595  
596  
597  
598  
599  
600  
601  
602  
603  
604  
605  
606  
607  
608  
609



610 **Figure 6.** Estimated annual average temperature at the top of Holtedahlfonna ice field (red dots)  
611 and the  $\delta^{18}\text{O}$  signal of the four shallow cores.  
612



613  
614  
615  
616  
617  
618  
619  
620  
621  
622  
623  
624  
625  
626  
627  
628  
629  
630  
631  
632  
633  
634  
635  
636



637 **TABLES**

638

639 **Table 1.** Shallow ice core descriptions. The table reports the length expressed in cm and in water  
640 equivalent (w.e.) and the estimated (Est. start year\Est. end year) time coverage. The average density  
641 of the cores is also reported.

642

Core ID	Length (cm)	Length (cm w.e.)	Ave density (kgL <sup>-1</sup> )	Est. Start year	Est. End year	Drilling period	Reference
2019	769	461	0.60	2018	2012	April 2019	This work
2017	736	466	0.63	2016	2010	April 2017	<i>Burgay et a. 2017</i>
2015	1185	832	0.70	2014	2005	May 2015	<i>Ruppel et al. 2017</i>
2012	954	575	0.60	2011	2004	April 2012	<i>Spolaor et al. 2013</i>

643

644

645

646

647

648

649

650

651

652

653

654

655

656

657

658

659

660

661

662

663

664

665

666

667

668

669

670

671

672

673

674

675

676

677

678

679

680



681 **REFERENCES**

- 682  
683 Arienzo, M. M., Legrand, M., Preunkert, S., Stohl, A., Chellman, N., Eckhardt, S., Gleason, K. E.,  
684 and McConnell, J. R.: Alpine Ice-Core Evidence of a Large Increase in Vanadium and Molybdenum  
685 Pollution in Western Europe During the 20th Century, *Journal of Geophysical Research: Atmospheres*, 126, <https://doi.org/10.1029/2020JD033211>, 2021.  
686  
687 Avak, S. E., Trachsel, J. C., Edebeli, J., Brütsch, S., Bartels-Rausch, T., Schneebeili, M.,  
688 Schwikowski, M., and Eichler, A.: Melt-Induced Fractionation of Major Ions and Trace Elements  
689 in an Alpine Snowpack, *J Geophys Res Earth Surf*, 124, 1647–1657,  
690 <https://doi.org/10.1029/2019JF005026>, 2019.  
691 Barbaro, E., Spolaor, A., Karroca, O., Park, K.-T., Martma, T., Isaksson, E., Kohler, J., Gallet, J. C.,  
692 Bjorkman, M. P., Cappelletti, D., Spreen, G., Zangrando, R., Barbante, C., and Gambaro, A.: Free  
693 amino acids in the Arctic snow and ice core samples: Potential markers for paleoclimatic studies,  
694 *Science of the Total Environment*, 607–608, <https://doi.org/10.1016/j.scitotenv.2017.07.041>, 2017.  
695 Beaudon, E., Moore, J. C., Martma, T., Pohjola, V. A., van de Wal, R. S. W., Kohler, J., and Isaksson,  
696 E.: Lomonosovfonna and Holtedahlfonna ice cores reveal east–west disparities of the Spitsbergen  
697 environment since <scp>AD</scp> 1700, *Journal of Glaciology*, 59, 1069–1083,  
698 <https://doi.org/10.3189/2013JoG12J203>, 2013.  
699 Beaudon, E., Moore, J. C., Martma, T., Pohjola, V. A., van de Wal, R. S. W., Kohler, J., and Isaksson,  
700 E.: Lomonosovfonna and Holtedahlfonna ice cores reveal east–west disparities of the Spitsbergen  
701 environment since AD 1700, *Journal of Glaciology*, 59, 1069–1083,  
702 <https://doi.org/10.3189/2013JoG12J203>, 2017.  
703 Bengtsson, L., Andrae, U., Aspelien, T., Batrak, Y., Calvo, J., de Rooy, W., Gleeson, E., Hansen-  
704 Sass, B., Homleid, M., Hortal, M., Ivarsson, K.-I., Lenderink, G., Niemelä, S., Nielsen, K. P.,  
705 Onvlee, J., Rontu, L., Samuelsson, P., Muñoz, D. S., Subias, A., Tijn, S., Toll, V., Yang, X., and  
706 Køltzow, M. Ø.: The HARMONIE–AROME Model Configuration in the ALADIN–HIRLAM  
707 NWP System, *Mon Weather Rev*, 145, 1919–1935, <https://doi.org/10.1175/MWR-D-16-0417.1>,  
708 2017.  
709 Boers, N.: Early-warning signals for Dansgaard-Oeschger events in a high-resolution ice core record,  
710 *Nat Commun*, 9, 2556, <https://doi.org/10.1038/s41467-018-04881-7>, 2018.  
711 Bohleber, P., Roman, M., Sala, M., Delmonte, B., Stenni, B., and Barbante, C.: Two-dimensional  
712 impurity imaging in deep Antarctic ice cores: snapshots of three climatic periods and implications  
713 for high-resolution signal interpretation, *Cryosphere*, 15, 3523–3538, <https://doi.org/10.5194/tc-15-3523-2021>, 2021.  
714  
715 Bonne, J.-L., Steen-Larsen, H. C., Risi, C., Werner, M., Sodemann, H., Lacour, J.-L., Fettweis, X.,  
716 Cesana, G., Delmotte, M., Cattani, O., Vallenga, P., Kjær, H. A., Clerbaux, C., Sveinbjörnsdóttir,  
717 Á. E., and Masson-Delmotte, V.: The summer 2012 Greenland heat wave: In situ and remote sensing  
718 observations of water vapor isotopic composition during an atmospheric river event, *Journal of Geophysical Research: Atmospheres*, 120, 2970–2989, <https://doi.org/10.1002/2014JD022602>,  
719 2015.  
720  
721 Burgay, F., Barbaro, E., Cappelletti, D., Turetta, C., Gallet, J.-C., Isaksson, E., Stenni, B., Dreossi,  
722 G., Scoto, F., Barbante, C., and Spolaor, A.: First discrete iron(II) records from Dome C (Antarctica)  
723 and the Holtedahlfonna glacier (Svalbard), *Chemosphere*, 267, 129335,  
724 <https://doi.org/https://doi.org/10.1016/j.chemosphere.2020.129335>, 2021.  
725 Dahe, Q., Mayewski, P. A., Wake, C. P., Shichang, K., Jiawen, R., Shugui, H., Tandong, Y., Qinzhaoh,  
726 Y., Zhefan, J., and Desheng, M.: Evidence for recent climate change from ice cores in the central  
727 Himalaya, *Ann Glaciol*, 31, 153–158, <https://doi.org/10.3189/172756400781819789>, 2000.  
728 Dahlke, S. and Maturilli, M.: Contribution of atmospheric advection to the amplified winter warming  
729 in the arctic north atlantic region, *Advances in meteorology*, <https://doi.org/10.1155/2017/4928620>,  
730 2017.



- 731 Dahlke, S., Hughes, N. E., Wagner, P. M., Gerland, S., Wawrzyniak, T., Ivanov, B., and Maturilli,  
732 M.: The observed recent surface air temperature development across Svalbard and concurring  
733 footprints in local sea ice cover, *International Journal of Climatology*, 40, 5246–5265,  
734 <https://doi.org/https://doi.org/10.1002/joc.6517>, 2020a.
- 735 Dahlke, S., Hughes, N. E., Wagner, P. M., Gerland, S., Wawrzyniak, T., Ivanov, B., and Maturilli,  
736 M.: The observed recent surface air temperature development across Svalbard and concurring  
737 footprints in local sea ice cover, *International Journal of Climatology*, n/a,  
738 <https://doi.org/10.1002/joc.6517>, 2020b.
- 739 Divine, D., Isaksson, E., Martma, T., Meijer, H. A. J., Moore, J., Pohjola, V., van de Wal, R. S. W.,  
740 and Godtlibsen, F.: Thousand years of winter surface air temperature variations in Svalbard and  
741 northern Norway reconstructed from ice-core data, *Polar Res*, 30, 7379,  
742 <https://doi.org/10.3402/polar.v30i0.7379>, 2011.
- 743 Førland, E. J., Isaksen, K., Lutz, J., Hanssen-Bauer, I., Schuler, T. V., Dobler, A., Gjelten, H. M., and  
744 Vikhamar-Schuler, D.: Measured and Modeled Historical Precipitation Trends for Svalbard, *J*  
745 *Hydrometeorol*, 21, 1279–1296, <https://doi.org/10.1175/JHM-D-19-0252.1>, 2020.
- 746 Gabrielli, P., Barbante, C., Bertagna, G., Bertó, M., Binder, D., Carton, A., Carturan, L., Cazorzi, F.,  
747 Cozzi, G., Dalla Fontana, G., Davis, M., de Blasi, F., Dinale, R., Dragà, G., Dreossi, G., Festi, D.,  
748 Frezzotti, M., Gabrieli, J., Galos, S. P., Ginot, P., Heidenwolf, P., Jenk, T. M., Kehrwald, N., Kenny,  
749 D., Magand, O., Mair, V., Mikhalenko, V., Lin, P. N., Oeggl, K., Piffer, G., Rinaldi, M., Schotterer,  
750 U., Schwikowski, M., Seppi, R., Spolaor, A., Stenni, B., Tonidandel, D., Uglietti, C., Zagorodnov,  
751 V., Zanoner, T., and Zennaro, P.: Age of the Mt. Ortles ice cores, the Tyrolean Iceman and glaciation  
752 of the highest summit of South Tyrol since the Northern Hemisphere Climatic Optimum,  
753 *Cryosphere*, 10, 2779–2797, <https://doi.org/10.5194/tc-10-2779-2016>, 2016.
- 754 Geyman, E. C., J. J. van Pelt, W., Maloof, A. C., Aas, H. F., and Kohler, J.: Historical glacier change  
755 on Svalbard predicts doubling of mass loss by 2100, *Nature*, 601, 374–379,  
756 <https://doi.org/10.1038/s41586-021-04314-4>, 2022.
- 757 Goto-Azuma, K., S. Kohshima, T., Kameda, S., Takahashi, O., Watanabe, Y. F., and Hagen., and J.  
758 O.: An ice-core chemistry record from Snøfjellafonna, northwestern Spitsbergen, *Ann. Glaciol.*, 21,  
759 213–218, 1995.
- 760 Hersbach, H., Bell, B., Berrisford, P., Hirahara, S., Horányi, A., Muñoz-Sabater, J., Nicolas, J.,  
761 Peubey, C., Radu, R., Schepers, D., Simmons, A., Soci, C., Abdalla, S., Abellan, X., Balsamo, G.,  
762 Bechtold, P., Biavati, G., Bidlot, J., Bonavita, M., Chiara, G., Dahlgren, P., Dee, D., Diamantakis,  
763 M., Dragani, R., Flemming, J., Forbes, R., Fuentes, M., Geer, A., Haimberger, L., Healy, S., Hogan,  
764 R. J., Hólm, E., Janisková, M., Keeley, S., Laloyaux, P., Lopez, P., Lupu, C., Radnoti, G., Rosnay,  
765 P., Rozum, I., Vamborg, F., Villaume, S., and Thépaut, J.: The ERA5 global reanalysis, *Quarterly*  
766 *Journal of the Royal Meteorological Society*, 146, 1999–2049, <https://doi.org/10.1002/qj.3803>,  
767 2020.
- 768 Hoffmann, G., Ramirez, E., Taupin, J. D., Francou, B., Ribstein, P., Delmas, R., Dürr, H., Gallaire,  
769 R., Simões, J., Schotterer, U., Stievenard, M., and Werner, M.: Coherent isotope history of Andean  
770 ice cores over the last century, *Geophys Res Lett*, 30, 2002GL014870,  
771 <https://doi.org/10.1029/2002GL014870>, 2003.
- 772 Isaksen, K., Nordli, Ø., Førland, E. J., Łupikasza, E., Eastwood, S., and Niedźwiedź, T.: Recent  
773 warming on Spitsbergen—Influence of atmospheric circulation and sea ice cover, *Journal of*  
774 *Geophysical Research: Atmospheres*, 121, 11, 911–913, 931,  
775 <https://doi.org/10.1002/2016JD025606>, 2016.
- 776 Isaksen, K., Nordli, Ø., Ivanov, B., Køltzow, M. A. Ø., Aaboe, S., Gjelten, H. M., Mezghani, A.,  
777 Eastwood, S., Førland, E., Benestad, R. E., Hanssen-Bauer, I., Brækkan, R., Sviashchennikov, P.,  
778 Demin, V., Revina, A., and Karandasheva, T.: Exceptional warming over the Barents area, *Sci Rep*,  
779 12, 9371, <https://doi.org/10.1038/s41598-022-13568-5>, 2022.
- 780 Isaksson, E., Hermanson, M., Hicks, S., Igarashi, M., Kamiyama, K., Moore, J., Motoyama, H., Muir,  
781 D., Pohjola, V., Vaikmäe, R., van de Wal, R. S. W., and Watanabe, O.: Ice cores from Svalbard—



- 782 useful archives of past climate and pollution history, *Physics and Chemistry of the Earth, Parts*  
783 *A/B/C*, 28, 1217–1228, <https://doi.org/10.1016/j.pce.2003.08.053>, 2003.
- 784 Isaksson, E., Kekonen, T., Moore, J., and Mulvaney, R.: The methanesulfonic acid (MSA) record in  
785 a Svalbard ice core, *Ann. Glaciol.*, 42, 345–351, 2005.
- 786 Kohler, J.: Mass balance for glaciers near Ny-Ålesund [Data set]. Norwegian Polar Institute, 2013.
- 787 Lind, S., Ingvaldsen, R. B., and Furevik, T.: Arctic warming hotspot in the northern Barents Sea  
788 linked to declining sea-ice import, *Nat Clim Chang*, 8, 634–639, [https://doi.org/10.1038/s41558-](https://doi.org/10.1038/s41558-018-0205-y)  
789 018-0205-y, 2018.
- 790 Matoba, S., Narita, H., Motoyama, H., Kamiyama, K., and Watanabe, O.: Ice core chemistry of  
791 Vestfonna Ice Cap in Svalbard, Norway, *Journal of Geophysical Research: Atmospheres*, 107, ACH  
792 19-1-ACH 19-7, <https://doi.org/10.1029/2002JD002205>, 2002.
- 793 Maturilli, M., Herber, A., and König-Langlo, G.: Climatology and time series of surface meteorology  
794 in Ny-Ålesund, Svalbard, *Earth Syst. Sci. Data*, 5, 155–163, [https://doi.org/10.5194/essd-5-155-](https://doi.org/10.5194/essd-5-155-2013)  
795 2013, 2013.
- 796 Noël, B., Jakobs, C. L., van Pelt, W. J. J., Lhermitte, S., Wouters, B., Kohler, J., Hagen, J. O., Luks,  
797 B., Reijmer, C. H., van de Berg, W. J., and van den Broeke, M. R.: Low elevation of Svalbard  
798 glaciers drives high mass loss variability, *Nat Commun*, 11, 4597, [https://doi.org/10.1038/s41467-](https://doi.org/10.1038/s41467-020-18356-1)  
799 020-18356-1, 2020.
- 800 Nuth, C., Schuler, T. V., Kohler, J., Altena, B., and Hagen, J. O.: Estimating the long-term calving  
801 flux of Kronebreen, Svalbard, from geodetic elevation changes and mass-balance modeling, *Journal*  
802 *of Glaciology*, 58, 119–133, <https://doi.org/10.3189/2012JoG11J036>, 2017.
- 803 Østby, T. I., Schuler, T. v., Hagen, J. O., Hock, R., Kohler, J., and Reijmer, C. H.: Diagnosing the  
804 decline in climatic mass balance of glaciers in Svalbard over 1957–2014, *Cryosphere*, 11, 191–215,  
805 <https://doi.org/10.5194/tc-11-191-2017>, 2017.
- 806 Peeters, B., Pedersen, Å. Ø., Loe, L. E., Isaksen, K., Veiberg, V., Stien, A., Kohler, J., Gallet, J.-C.,  
807 Aanes, R., and Hansen, B. B.: Spatiotemporal patterns of rain-on-snow and basal ice in high Arctic  
808 Svalbard: detection of a climate-cryosphere regime shift, *Environmental Research Letters*, 14,  
809 015002, <https://doi.org/10.1088/1748-9326/aaefb3>, 2019.
- 810 van Pelt, W. J. J., Kohler, J., Liston, G. E., Hagen, J. O., Luks, B., Reijmer, C. H., and Pohjola, V.  
811 A.: Multidecadal climate and seasonal snow conditions in Svalbard, *J Geophys Res Earth Surf*, 121,  
812 2100–2117, <https://doi.org/https://doi.org/10.1002/2016JF003999>, 2016.
- 813 van Pelt, W., Pohjola, V., Pettersson, R., Marchenko, S., Kohler, J., Luks, B., Hagen, J. O., Schuler,  
814 T. v., Dunse, T., Noël, B., and Reijmer, C.: A long-term dataset of climatic mass balance, snow  
815 conditions, and runoff in Svalbard (1957–2018), *Cryosphere*, 13, 2259–2280,  
816 <https://doi.org/10.5194/tc-13-2259-2019>, 2019.
- 817 Pohjola, V. A., Moore, J. C., Isaksson, E., Jauhiainen, T., Van de Wal, R. S. W., Martma, T., Meijer,  
818 H. A. J., and Vaikmäe, R.: Effect of periodic melting on geochemical and isotopic signals in an ice  
819 core from Lomonosovfonna, Svalbard, *J. Geophys. Res. Atmos.*, 107, 1–14, 2002.
- 820 Rantanen, M., Karpechko, A. Yu., Lipponen, A., Nordling, K., Hyvärinen, O., Ruosteenoja, K.,  
821 Vihma, T., and Laaksonen, A.: The Arctic has warmed nearly four times faster than the globe since  
822 1979, *Commun Earth Environ*, 3, 168, <https://doi.org/10.1038/s43247-022-00498-3>, 2022a.
- 823 Rantanen, M., Karpechko, A. Yu., Lipponen, A., Nordling, K., Hyvärinen, O., Ruosteenoja, K.,  
824 Vihma, T., and Laaksonen, A.: The Arctic has warmed nearly four times faster than the globe since  
825 1979, *Commun Earth Environ*, 3, 168, <https://doi.org/10.1038/s43247-022-00498-3>, 2022b.
- 826 Ruppel, M. M., Soares, J., Gallet, J.-C., Isaksson, E., Martma, T., Svensson, J., Kohler, J., Pedersen,  
827 C. A., Manninen, S., Korhola, A., and Ström, J.: Do contemporary (1980–2015) emissions  
828 determine the elemental carbon deposition trend at Holtedahlfonna glacier, Svalbard?, *Atmos Chem*  
829 *Phys*, 17, 12779–12795, <https://doi.org/10.5194/acp-17-12779-2017>, 2017.
- 830 Schuler, T. v., Kohler, J., Elagina, N., Hagen, J. O. M., Hodson, A. J., Jania, J. A., Kääh, A. M., Luks,  
831 B., Mafecki, J., Moholdt, G., Pohjola, V. A., Sobota, I., and van Pelt, W. J. J.: Reconciling Svalbard  
832 Glacier Mass Balance, *Front Earth Sci (Lausanne)*, 8, 2020.



- 833 Schwikowski, M., Döscher, A., Gäggeler, H. W., and Schotterer, U.: Anthropogenic versus natural  
834 sources of atmospheric sulphate from an Alpine ice core, *Tellus B: Chemical and Physical*  
835 *Meteorology*, 51, 938, <https://doi.org/10.3402/tellusb.v51i5.16506>, 1999.
- 836 Schyberg, H., Yang, X., Koltzow, M., Amstrup, B., Bakketun, B., Bazile, E., Bojarova, J., Box,  
837 J., Dahlgren, P., Hagelin, S., Homleid, M., Horanyi, A., Hoyer, J., Johansson, K. M., Kornich,  
838 H., le Moigne, P., Lindskog, M., Manninen, T., Nielsen Englyst, P., and Wang, Z.: Arctic  
839 regional reanalysis on single levels from 1991 to present, , 2020.
- 840 Scoto, F., Sadatzki, H., Maffezzoli, N., Barbante, C., Gagliardi, A., Varin, C., Vallelonga, P., Gkinis,  
841 V., Dahl-Jensen, D., Kjær, H. A., Burgay, F., Saiz-Lopez, A., Stein, R., and Spolaor, A.: Sea ice  
842 fluctuations in the Baffin Bay and the Labrador Sea during glacial abrupt climate changes,  
843 *Proceedings of the National Academy of Sciences*, 119, e2203468119,  
844 <https://doi.org/10.1073/pnas.2203468119>, 2022.
- 845 Sobota, I., Weckwerth, P., and Grajewski, T.: Rain-On-Snow (ROS) events and their relations to  
846 snowpack and ice layer changes on small glaciers in Svalbard, the high Arctic, *J Hydrol (Amst)*,  
847 590, 125279, <https://doi.org/https://doi.org/10.1016/j.jhydrol.2020.125279>, 2020.
- 848 Spolaor, A., Gabrieli, J., Martma, T., Kohler, J., Björkman, M. B., Isaksson, E., Varin, C., Vallelonga,  
849 P., Plane, J. M. C., and Barbante, C.: Sea ice dynamics influence halogen deposition to Svalbard,  
850 *Cryosphere*, 7, 1645–1658, <https://doi.org/10.5194/tc-7-1645-2013>, 2013a.
- 851 Spolaor, A., Gabrieli, J., Martma, T., Kohler, J., Björkman, M. B., Isaksson, E., Varin, C., Vallelonga,  
852 P., Plane, J. M. C., and Barbante, C.: Sea ice dynamics influence halogen deposition to Svalbard,  
853 *Cryosphere*, 7, 1645–1658, <https://doi.org/10.5194/tc-7-1645-2013>, 2013b.
- 854 Spolaor, A., Barbante, C., Cairns, W. R. L., and Boutron, C.: Man’s footprint on the Arctic  
855 environment as revealed by analysis of ice and snow, *Earth Sci Rev*,  
856 <https://doi.org/10.1016/j.earscirev.2017.02.010>, 2016.
- 857 Spolaor, A., Varin, C., Pedeli, X., Christille, J. M., Kirchgeorg, T., Giardi, F., Cappelletti, D., Turetta,  
858 C., Cairns, W. R. L., Gambaro, A., Bernagozzi, A., Gallet, J. C., Björkman, M. P., and Barbaro, E.:  
859 Source, timing and dynamics of ionic species mobility in the Svalbard annual snowpack, *Science*  
860 *of The Total Environment*, 751, 141640,  
861 <https://doi.org/https://doi.org/10.1016/j.scitotenv.2020.141640>, 2021.
- 862 Steffensen, J. P., Andersen, K. K., Bigler, M., Clausen, H. B., Dahl-Jensen, D., Fischer, H., Goto-  
863 Azuma, K., Hansson, M., Johnsen, S. J., Jouzel, J., Masson-Delmotte, V., Popp, T., Rasmussen, S.  
864 O., Röthlisberger, R., Ruth, U., Stauffer, B., Siggaard-Andersen, M.-L., Sveinbjörnsdóttir, Á. E.,  
865 Svensson, A., and White, J. W. C.: High-Resolution Greenland Ice Core Data Show Abrupt Climate  
866 Change Happens in Few Years, *Science* (1979), 321, 680–684, 2008.
- 867 Steffensen Schmidt, L., Schuler, T. V., Thomas, E. E., and Westermann, S.: Meltwater runoff and  
868 glacier mass balance in the high Arctic: 1991–2022 simulations for Svalbard, *EGUsphere*, 2023, 1–  
869 32, <https://doi.org/10.5194/egusphere-2022-1409>, 2023.
- 870 Stenni, B., Curran, M. A. J., Abram, N. J., Orsi, A., Goursaud, S., Masson-Delmotte, V., Neukom,  
871 R., Goosse, H., Divine, D., van Ommen, T., Steig, E. J., Dixon, D. A., Thomas, E. R., Bertler, N.  
872 A. N., Isaksson, E., Ekaykin, A., Werner, M., and Frezzotti, M.: Antarctic climate variability on  
873 regional and continental scales over the last 2000 years, *Clim. Past*, 13, 1609–1634,  
874 <https://doi.org/10.5194/cp-13-1609-2017>, 2017.
- 875 Thompson, L. G., Yao, T., Davis, M. E., Mosley-Thompson, E., Wu, G., Porter, S. E., Xu, B., Lin,  
876 P.-N., Wang, N., Beaudon, E., Duan, K., Sierra-Hernández, M. R., and Kenny, D. v.: Ice core  
877 records of climate variability on the Third Pole with emphasis on the Guliya ice cap, western Kunlun  
878 Mountains, *Quat Sci Rev*, 188, 1–14, <https://doi.org/10.1016/j.quascirev.2018.03.003>, 2018.
- 879 Vance, T. R., Roberts, J. L., Moy, A. D., Curran, M. A. J., Tozer, C. R., Gallant, A. J. E., Abram, N.  
880 J., van Ommen, T. D., Young, D. A., Grima, C., Blankenship, D. D., and Siegert, M. J.: Optimal  
881 site selection for a high-resolution ice core record in East Antarctica, *Climate of the Past*, 12, 595–  
882 610, <https://doi.org/10.5194/cp-12-595-2016>, 2016.

